Guided ion beam studies of the reactions of Ni_n^+ ($n=2-18$) with O_2: Nickel cluster oxide and dioxide bond energies

Dinesh Vardhan
Department of Chemical & Fuels Engineering, University of Utah, Salt Lake City, Utah 84112

Rohana Liyanage
Statewide Mass Spectrometry Facility, University of Arkansas, Fayetteville, Arkansas 72701

P. B. Armentrout
Department of Chemistry, University of Utah, Salt Lake City, Utah 84112

(Received 23 April 2003; accepted 27 May 2003)

The kinetic energy dependences of the reactions of Ni_n^+ ($n=2-18$) with O_2 are studied in a guided ion beam tandem mass spectrometer. A variety of $Ni_mO_2^+$, Ni_mO^+, and Ni_m^+ product ions, where $m \leq n$, are observed, with the dioxide cluster ions dominating the products for all larger reactant cluster ions. Reaction efficiencies are near unity for all but the smallest clusters. The energy dependences of the product cross sections are analyzed in several different ways to determine thermochemistry for both the first and second oxygen atom binding to nickel cluster ions. These values show little dependence on cluster size for clusters larger than three atoms. The trends in this thermochemistry are discussed and compared to bulk phase oxidation values. © *2003 American Institute of Physics.* [DOI: 10.1063/1.1592502]

I. INTRODUCTION

Oxidation of nickel and its alloys is a subject of considerable interest because of its importance in corrosion and catalysis. The properties of nickel alloys, which make them of industrial importance, are varied. These properties include good corrosion resistance to many gaseous and liquid environments at normal temperatures, resistance to oxidation at elevated temperatures, and good mechanical strength at high temperatures. Nickel plating is often used to provide a protective coating for other metals. There are various types of steel and corrosion-resistant alloys that include carbon and nickel for hardness. Therefore understanding the energetics of the oxidation of nickel is of some industrial importance as well as being of fundamental interest. Studying this oxidation process with gas-phase clusters of nickel can provide quantitative data concerning the elementary steps that make up the complicated surface processes and thus help us understand surface science at a molecular level. Studies of the chemical reactivity, magnetic properties, electronic structures, and geometric structure of transition metal clusters are currently an active frontier in chemical physics.[1–10]

The oxidation of neutral nickel clusters with O_2 has been studied in a fast flow tube reactor where the products are detected by multiphoton ionization and time-of-flight mass spectrometry. In the experimental setup of Riley and co-workers,[11] oxygen was admitted to the flow reactor downstream of the cluster formation region. They found that initial stages of oxidation favored formation of cluster dioxides, Ni_nO_2, with little or no increase in the intensity of Ni_nO products, presumably formed in the laser vaporization plasma. The efficiency of the dioxide formation reactions was estimated to be close to unity. They observed that oxide ion compositions rapidly assume a constant oxygen to metal ratio with increasing cluster size. For clusters $n>10$, it was found that the oxygen/metal ratio was approximately 0.75, with a slight decrease in this ratio with increasing cluster size. In related work, Castleman and co-workers have also examined the oxidation reactions of charged nickel and nickel oxide clusters (cations and anions) with NO and NO_2 at thermal energies and under multiple collision conditions.[12–15]

There have been many studies of the oxidation of nickel surfaces.[16] This work establishes that the oxidation of a Ni surface proceeds in three sequential regimes; dissociative chemisorption, in which surface reconstruction takes place, followed by oxide nucleation and coalescence, and in-depth oxide growth. Little thermochemical information is available from this work because the surfaces reconstruct upon oxidation, thereby making quantification of the energetics difficult. Calorimetry studies on the nickel 111 surface find that desorption of molecular oxygen requires 4.86 eV.[17] More recent calorimetry studies find desorption enthalpies of 4.6 eV for Ni(111), 4.9 eV for Ni(110), and 5.7 eV for Ni(100), all measured for the low coverage regime.[18] These studies also demonstrate that the desorption enthalpies decrease with increasing coverage.

In the present work, we examine the reactions of nickel cluster cations, Ni_n^+ ($n=2-18$) with oxygen. This extends our growing database of studies of clusters of transition metal cations[19–28] and their reactions with O_2,[29–31] CO_2,[32,33] D_2,[34–37] and CD_4.[38,39] The quantitative thermochemistry data regarding the stability of the bare nickel clusters previously measured in our laboratories provide insight into the geometric structures and dissociation pathways.[25] In contrast to the flow reactor studies that examine reactions only at thermal energies, the kinetic energy dependence of these reactions over a wide range is studied here using guided ion

beam tandem mass spectrometry. Our reactivity results at thermal energies should parallel the observations for neutral nickel clusters. However, by analyzing the kinetic energy dependences of these processes, we are able to obtain quantitative data regarding the thermodynamics of the oxidation reactions. The trends in this information are discussed in some detail and compared with bulk phase thermochemistry.

II. EXPERIMENT

Reactions of nickel cluster cations with O_2 are studied using a guided ion beam tandem mass spectrometer equipped with a laser ablation cluster source. The experimental apparatus and techniques used in this work have been described in detail elsewhere.[40,41] A copper vapor laser (Oxford ACL-35, 511 and 578 nm, 7 kHz repetition rate, 3–4 mJ/pulse) is tightly focused onto a rotating and translating nickel rod. The plasma thus created is entrained in a continuous flow of helium at a flow rate between 5000 and 6000 sccm. The helium is passed through a liquid N_2 cooled molecular sieve trap to remove impurities. Clustering of the nickel atoms and ions occurs in a 2 mm diameter, 6.3 cm long condensation tube that immediately follows the target. An average ion undergoes approximately 10^5 collisions with He in this channel, a number that should be sufficient to equilibrate the ions to the temperature of the He carrier gas. The gas mixture expands from the clustering channel into the source chamber in a mild supersonic expansion that further cools the internal modes of the clusters. Nickel cluster ions thus created are therefore believed to be fully thermalized and may be cooler. The region between the vaporization block and the skimmer is kept field free and the focusing lenses in the two differential regions that follow are also kept at low potentials so that collisional reheating of the cluster ions is minimized.

The nickel cluster ions are extracted from the source, focused into a magnetic sector for mass analysis, decelerated to a desired kinetic energy, and focused into an rf octopole ion beam guide.[42] Reactions take place within the octopole where the neutral gas (O_2) is introduced. The octopole beam guide utilizes rf electric fields to create a potential well that traps ions in the transverse direction without affecting their axial energy. Product and unreacted cluster ions drift out of the collision chamber to the end of the octopole, where they are extracted and focused into a quadrupole mass filter for mass analysis. The quadrupole has a mass limit of ~1100 amu such that nickel cluster reaction products up to $Ni_{18}O_2^+$ can be studied. Finally, ions are detected by a 27 kV conversion dynode, secondary electron scintillation ion counter,[43] and the signal is processed using standard counting techniques. Conversion of detected ion intensities into reaction cross sections is treated as discussed previously.[41] Absolute cross sections measured in our laboratory have an uncertainty estimated as ±30% and relative uncertainties of ±5%.

Laboratory ion energies (lab) are converted to energies in the center-of-mass frame (CM) by using $E(\mathrm{CM}) = E(\mathrm{lab})M/(M+m)$, where m is the cluster ion mass and M is the mass of dioxygen (32.00 amu). Unless stated otherwise, all energies quoted in this paper correspond to the CM frame. The absolute energy scale and the corresponding full width at half maximum (FWHM) of the ion kinetic energy distribution are determined by using the octopole ion beam guide as a retarding energy analyzer. The uncertainty in the absolute energy scale is ±0.05 eV (lab) and the widths range from 0.7 to 2.3 eV, increasing with cluster size.

TABLE I. Bond energies and ionization energies from the literature (eV).[a]

Species	D_0	IE
Ni	···	7.6398[b]
Ni_2	2.068(0.01)[c]	7.63(0.07)[d]
Ni_2^+	2.08(0.07)[d]	···
NiO	3.91(0.17)[e]	8.77(0.18)[f]
Ni^+–O	2.75(0.05)[f]	···
Ni_2–O	4.38[g]	···
O_2	5.116(0.002)[h]	12.071[h]
O	···	13.619[h]

[a]Uncertainties given in parentheses.
[b]Reference 46.
[c]Reference 47.
[d]Reference 25.
[e]Reference 48.
[f]Reference 45.
[g]Reference 49.
[h]Reference 50.

III. RESULTS

The reactions were carried out from thermal energies to 10 eV in the center-of-mass frame. As a general nomenclature, we will refer to $Ni_mO_2^+$ products as "cluster dioxides," Ni_mO^+ products as "cluster monoxides," and Ni_m^+ products as "cluster fragments," where $m \leq n$ for reaction of Ni_n^+. A complete set of figures for all Ni_n^+ clusters (n=2–18) reacting with O_2 can be obtained from Ref. 44. Reaction of atomic Ni^+ with O_2 has been studied previously.[45] Thermochemistry used to determine some of the threshold energies for the smallest clusters is listed in Table I.[46–50] Throughout the text, thermochemistry for the bare cluster dissociation energies is obtained from Ref. 25.

In all of these systems, there are two difficulties in obtaining reliable cross section data. First, in order to efficiently collect all products throughout the energy range of interest (0–10 eV CM), the resolution of the quadrupole mass filter is set fairly low, but this leads to overlap of adjacent mass peaks. Because most of the energy dependences of the various products are usually quite distinct, such overlap is easily identified and eliminated. The cross sections shown here have been corrected for such problems as long as the corrections are unambiguous. Second, the more intense products formed in a single bimolecular collision between the nickel cluster ion and O_2 can react with O_2 again to form higher order cluster oxide products. These can be identified easily by their mass and by examining the pressure dependence of the cross sections. In the present system, we verified the energy dependences of the cross sections were not affected by the pressure of the reactant gas. The absolute magnitudes of the primary reaction products are affected by less than the 20% absolute uncertainty in the absolute magnitudes. On the basis of such studies, the cross sections shown in the paper correspond to single reactive collisions.

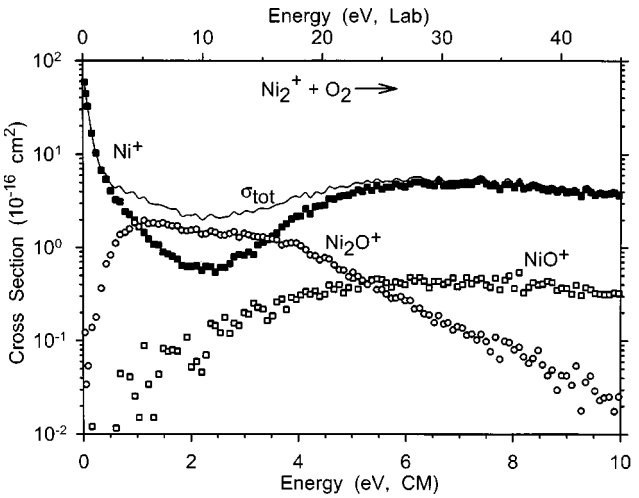

FIG. 1. Cross section for the reaction of Ni_2^+ with O_2 as a function of collision energy in the center-of-mass (lower x axis) and laboratory (upper x axis) frames.

A. $Ni_2^+ + O_2$

In the reaction of nickel dimer cation with O_2, there are five possible metal containing ionic products: $Ni_2O_2^+$, Ni_2O^+, NiO_2^+, NiO^+, and Ni^+. Only Ni_2O^+, NiO^+, and Ni^+ are observed, as shown in Fig. 1. O_2^+ and O^+ ions are not observed in the reactions of this or any other cluster size because the ionization energies of O_2 and O are much higher than of any nickel containing products, Table I. For the three product ions that are observed, there are seven possible *pathways* for this system, reactions (1)–(7). Reaction enthalpies at 0 K (with uncertainties in parentheses) are indicated for all reactions where the thermochemical information is known from literature data (see Table I and Ref. 25).

$$Ni_2^+ + O_2 \rightarrow Ni_2O^+ + O \quad (1)$$

$$\rightarrow NiO^+ + NiO \quad 0.54(0.18) \quad (2)$$

$$\rightarrow NiO^+ + Ni + O \quad 4.45(0.07) \quad (3)$$

$$\rightarrow Ni^+ + NiO_2 \quad <0 \quad (4)$$

$$\rightarrow Ni^+ + Ni + O_2 \quad 2.08(0.07) \quad (5)$$

$$\rightarrow Ni^+ + NiO + O \quad 3.28(0.18) \quad (6)$$

$$\rightarrow Ni^+ + Ni + 2O \quad 7.19(0.07). \quad (7)$$

There is only one reaction pathway, process (1), for the formation of Ni_2O^+, explaining why there is a single feature to the cross section over the entire energy range. The Ni_2O^+ cross section rises rapidly with energy from a nonzero cross section at the lowest kinetic energies, suggesting that process (1) is slightly endothermic. It reaches a plateau above 1 eV, and then above about 4 eV, the Ni_2O^+ cross section declines, corresponding with an increase in the Ni^+ cross section. This behavior indicates that Ni_2O^+ is decomposing to $Ni^+ + NiO$, which corresponds to the overall reaction (6). Note that this pathway is favored over decomposition to $Ni + NiO^+$, reaction (3). NiO^+ displays a prominent endothermic feature, consistent with reaction (2), with no obvious increase at the threshold energy for reaction (3).

The dominant product over the most of the energy range examined is the Ni^+ fragment, which displays the most complicated energy dependence because there are four possible pathways to form this ion. Reaction (4) is the only pathway to which the exothermic portion of this cross section can be attributed. Such behavior can often be quantified by the Langevin–Gioumousis–Stevenson (LGS)[51] formula, $\sigma_{LGS} = \pi e(2\alpha/E)^{1/2}$ where α is the polarizability of O_2 (1.57 Å^3),[52] e is the charge on the electron, and E is the kinetic energy. We find that the total cross section follows $0.5\,\sigma_{LGS}$ from thermal energies to 0.1 eV before dropping to about $0.15\,\sigma_{LGS}$ from 0.25 to 1.5 eV. The rise in the Ni^+ cross section is coupled with the decrease in the Ni_2O^+ cross section and can be attributed in part to reaction (6). It seems likely that reaction (5), simple collision-induced dissociation (CID) also contributes to the formation of the Ni^+ product observed. The CID cross section of Ni_2^+ with Xe[25] has a comparable magnitude to the Ni^+ cross section observed here at high energies. Formation of $NiO_2^+ + Ni$, not observed here, is the least probable product channel, unlike the larger cluster ions where cluster dioxides are major ionic products.

B. $Ni_3^+ + O_2$

In the reaction of the nickel trimer cation with O_2, five product ions are observed, several of which exhibit multiple features, Fig. 2. For these product ions, there are 20 reaction pathways, reactions (8)–(12), that are accessible. Reaction enthalpies at 0 K are based on information from Table I and Ref. 25.

$$Ni_3^+ + O_2 \rightarrow Ni_3O^+ + O \quad >0 \quad (8)$$

$$\rightarrow Ni_2O^+ + NiO \quad <0 \quad (9a)$$

$$\rightarrow Ni_2O^+ + Ni + O \quad >0 \quad (9b)$$

$$\rightarrow Ni_2^+ + NiO_2 \quad <0 \quad (10a)$$

$$\rightarrow Ni_2^+ + Ni + O_2 \quad 2.36(0.12) \quad (10b)$$

$$\rightarrow Ni_2^+ + NiO + O \quad 3.56(0.21) \quad (10c)$$

$$\rightarrow Ni_2^+ + Ni + 2O \quad 7.47(0.12) \quad (10d)$$

$$\rightarrow NiO^+ + Ni_2O \quad 0.35(0.13) \quad (11a)$$

$$\rightarrow NiO^+ + NiO + Ni \quad 2.90(0.22) \quad (11b)$$

$$\rightarrow NiO^+ + Ni_2 + O \quad 4.73(0.12) \quad (11c)$$

$$\rightarrow NiO^+ + 2Ni + O \quad 6.81(0.15) \quad (11d)$$

$$\rightarrow Ni^+ + Ni_2O_2 \quad <0 \quad (12a)$$

$$\rightarrow Ni^+ + Ni + NiO_2 \quad >0 \quad (12b)$$

$$\rightarrow Ni^+ + 2NiO \quad 1.73(0.28) \quad (12c)$$

$$\rightarrow Ni^+ + Ni_2 + O_2 \quad 2.37(0.14) \quad (12d)$$

$$\rightarrow Ni^+ + Ni_2O + O \quad 3.10(0.14) \quad (12e)$$

$$\rightarrow Ni^+ + 2Ni + O_2 \quad 4.44(0.14) \quad (12f)$$

$$\rightarrow Ni^+ + Ni + NiO + O \quad 5.64(0.22) \quad (12g)$$

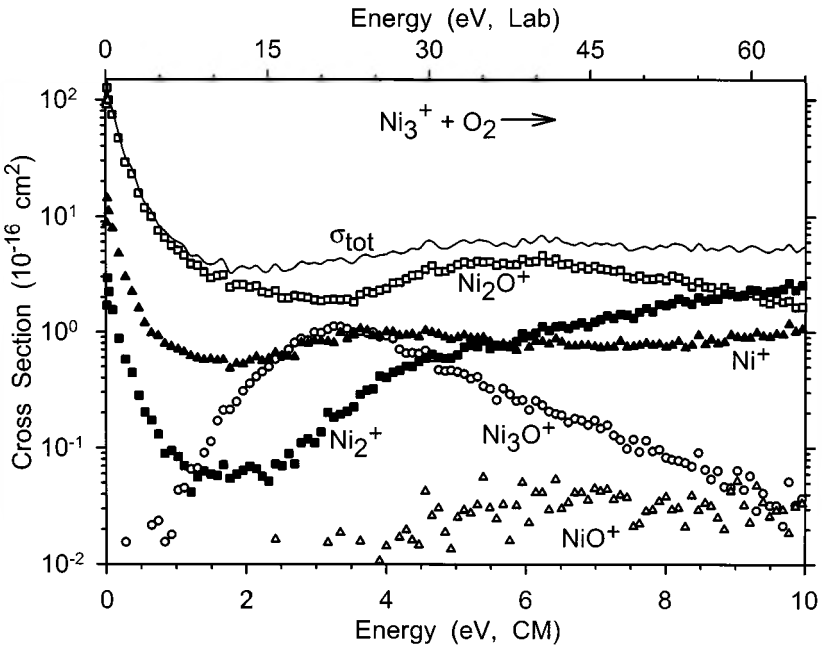

FIG. 2. Cross section for the reaction of Ni_3^+ with O_2 as a function of collision energy in the center-of-mass (lower x axis) and laboratory (upper x axis) frames.

$$\rightarrow Ni^+ + Ni_2 + 2O \quad 7.47(0.12) \qquad (12h)$$

$$\rightarrow Ni^+ + 2Ni + 2O \quad 9.55(0.14). \qquad (12i)$$

Well within experimental error, the total cross section for the reaction of nickel trimer cation with oxygen equals σ_{LGS} at thermal energies and up to 0.2 eV, before falling off more rapidly with energy. Among the cluster monoxide products, Fig. 2, the dominant product at all energies is Ni_2O^+, which is formed at low energies in the overall reaction (9a). A second feature beginning at about 3.5 eV must be the result of reaction (9b), which occurs by Ni atom loss from Ni_3O^+. This primary product ion can be formed in only one path, reaction (8), which is endothermic. The Ni_3O^+ cross section reaches a maximum near 3.5 eV, verifying that this product decomposes to $Ni_2O^+ + Ni$.

NiO^+ displays an endothermic cross section with an apparent threshold most consistent with reaction (11b). Reaction (11b) corresponds to decomposition of the Ni_2O^+ product formed in reaction (9a) into $NiO^+ + Ni$. As in Fig. 1, this decomposition competes with formation of $Ni^+ + NiO$, reaction (12c). This latter pathway is thermodynamically favored, consistent with the larger cross section of Ni^+ versus NiO^+ at high collision energies.

Metal fragments are also observed as products, Fig. 2. The Ni^+ product reaches a magnitude of 15 Å^2 at thermal energies with a complicated energy dependence including an exothermic feature that must be attributed to reaction (12a). On the basis of the discussion above, reaction (12c) surely contributes to the endothermic feature beginning near 2 eV. It is also possible that reaction (12d) also contributes, but CID with Xe exhibits a Ni^+ cross section smaller than Ni_2^+ at all energies.[25] The exothermic feature in the Ni_2^+ cross section must be a result of reaction (10a) and the second feature starting near 2 eV corresponds primarily to reaction (10b), the simple CID process. The magnitude of the Ni_2^+ cross section at the highest energies is about half of that observed in CID of Ni_3^+ with Xe.[25] Although contributions from reaction (10c) cannot be excluded definitively, this reaction requires a primary precursor product ion of either Ni_3O^+, which loses NiO, or Ni_2O^+, which loses an oxygen atom. The Ni_3O^+ precursor appears to dissociate primarily to $Ni_2O^+ + Ni$ and oxygen atom loss from Ni_2O^+ seems improbable as it is the highest energy decomposition pathway for this species.

C. $Ni_4^+ + O_2$

As the number of atoms, n, in the reactant cluster ion increases, the number of metal-containing products possible for the cluster systems grows as $3n-1$ and the number of product formation pathways grows much more rapidly. The Ni_4^+ system can produce 11 different product ions containing Ni and there are at least 49 possible reaction pathways. Figure 3 shows the product cross sections observed in the reaction of Ni_4^+ with O_2. Seven of the 11 possible products are observed (all but $Ni_4O_2^+$, $Ni_2O_2^+$, NiO_2^+, and NiO^+). As it is laborious to list all the reaction pathways for larger clusters, we shall do so only for the reactions observed, excluding simple CID:

$$Ni_4^+ + O_2 \rightarrow Ni_3O_2^+ + Ni \qquad (13)$$

$$\rightarrow Ni_4O^+ + O \qquad (14)$$

$$\rightarrow Ni_3O^+ + NiO \qquad (15a)$$

$$\rightarrow Ni_3O^+ + Ni + O \qquad (15b)$$

$$\rightarrow Ni_2O^+ + Ni_2O \qquad (16a)$$

$$\rightarrow Ni_2O^+ + NiO + Ni \qquad (16b)$$

$$\rightarrow Ni_2O^+ + 2Ni + O \qquad (16c)$$

$$\rightarrow Ni^+ + Ni_3O_2 \qquad (17a)$$

$$\rightarrow Ni^+ + Ni_2O_2 + Ni. \qquad (17b)$$

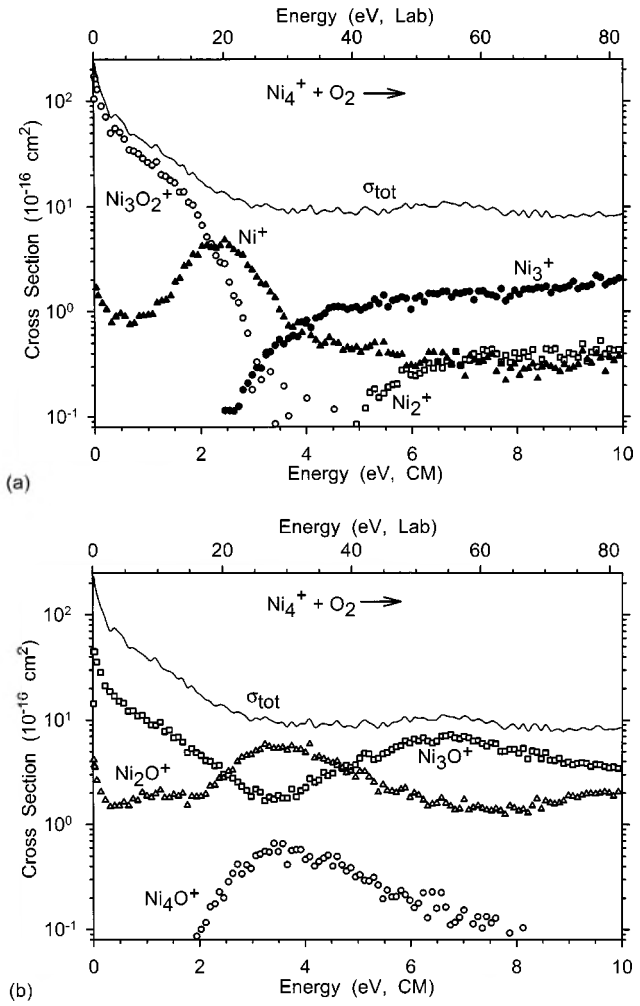

FIG. 3. Cross section for the reaction of Ni_4^+ with O_2 as a function of collision energy in the center-of-mass (lower x axis) and laboratory (upper x axis) frames. Part (a) exhibits the cluster dioxide and the cluster fragment products. Part (b) shows the cluster monoxide products.

Many of these cross sections display complicated energy dependences. The only cluster dioxide product formed, Fig. 3(a), is the $Ni_3O_2^+$ product, which can be formed in only a single pathway, accompanied by atomic Ni, corresponding to reaction (13). The cross section behaves as an exothermic reaction, declining with energy as $E^{-1/2}$ until 1 eV, in agreement with the behavior of the LGS cross section. The magnitude measured here is somewhat larger than this collision cross section, by about 50%. Above about 2 eV, the $Ni_3O_2^+$ product cross section declines even faster, indicating the onset of dissociation. On the basis of the results for the $Ni_3^+ + O_2$ system, it is clear that $Ni_3O_2^+$ dissociates preferentially by losing NiO to form Ni_2O^+, reaction (16b), and also by Ni^+ loss yielding Ni_2O_2, reaction (17b). Both the Ni_2O^+ and Ni^+ product cross sections exhibit endothermic features that are consistent with such decompositions. Exothermic formation of Ni^+ must be associated with reaction (17a).

The energy dependence for Ni_3^+ formation is consistent with the simple CID process, which has a threshold of 1.94 ± 0.15 eV.[25] The cross section rises more slowly from threshold compared to the CID studies with Xe, and the magnitude at higher energies is about half.[25] It seems likely that simple CID with a threshold of 4.31 ± 0.19 eV produces Ni_2^+, Fig. 3(a).

Figure 3(b) displays the monoxide products formed in this system. The primary Ni_4O^+ product can only be formed along one endothermic pathway, reaction (14). The exothermic feature in the Ni_3O^+ cross section must correspond to formation of a NiO neutral, reaction (15a), and the endothermic feature to Ni+O formation, reaction (15b). This latter path is equivalent to dissociation of Ni_4O^+ by Ni atom loss. The correspondence of the peaks in the Ni_4O^+ cross section and the onset of the endothermic feature in the Ni_3O^+ confirms this. The Ni_3O^+ product formed by both pathways can then dissociate by loss of a Ni atom at still higher energies. This contributes to the low energy endothermic feature in the Ni_2O^+ cross section, reaction (16b), and at very high energies, reaction (16c). The cross section for Ni_2O^+ also has an exothermic feature that must therefore correspond to formation of $Ni_2O^+ + Ni_2O$, reaction (16a).

D. $Ni_5^+ + O_2$

The product cross sections for reaction of Ni_5^+ with O_2 are shown in Fig. 4. Eight of 14 possible product ions containing Ni are observed. The dioxide products dominate the products at low energies and the monoxides dominate at higher energies. Of the cluster dioxide products, the $Ni_4O_2^+$ product can be formed in only a single pathway, accompanied by atomic Ni. The $Ni_4O_2^+ + Ni$ channel is the dominant low energy product and has a cross section with an energy dependence comparable to the σ_{LGS} limit up to about 1 eV, and a magnitude that is again somewhat larger. The cross section of $Ni_4O_2^+$ behaves as an exothermic reaction and then declines more rapidly with energy as the $Ni_3O_2^+$ cross section rises. This clearly indicates that $Ni_4O_2^+$ decomposes by Ni atom loss. Simple CID to form Ni_4^+ can begin at 2.07 ± 0.15 eV[25] and accounts for the major feature in the Ni_4^+ cross section. The energy dependence for Ni_3^+ formation is consistent with the simple CID process, which has a threshold of 2.01 ± 0.27 eV.[25]

For the cluster monoxide product ions, Fig. 4(b), Ni_5O^+ is formed in an endothermic reaction along with O. Most of the Ni_4O^+ cross section must correspond to the formation of Ni+O neutrals because the cross section rises as the Ni_5O^+ falls. Ni_3O^+ is the dominant monoxide product from the lowest energies to about 4.0 eV. The Ni_3O^+ cross section appears to have three distinct features that could result from reactions (18a)–(18d).

$$Ni_5^+ + O_2 \rightarrow Ni_3O^+ + Ni_2O \quad (18a)$$

$$\rightarrow Ni_3O^+ + Ni_2 + O \quad (18b)$$

$$\rightarrow Ni_3O^+ + NiO + Ni \quad (18c)$$

$$\rightarrow Ni_3O^+ + 2Ni + O. \quad (18d)$$

The exothermic portion of this cross section must be a result of reaction (18a). The lowest energy endothermic feature is probably a result of reaction (18c), because $Ni_4O_2^+$ was shown to decompose efficiently to both $Ni_3O_2^+ + Ni$ and to $Ni_3O^+ + NiO$ in the reactions of the tetramer, Fig. 3. The

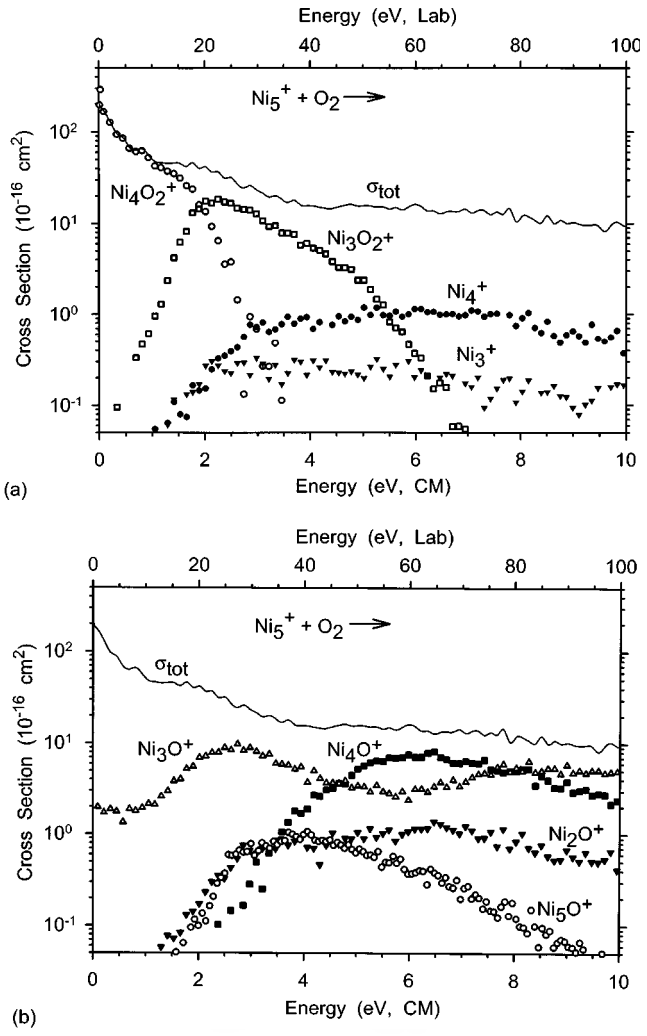

FIG. 4. Cross section for the reaction of Ni_5^+ with O_2 as a function of collision energy in the center-of-mass (lower x axis) and laboratory (upper x axis) frames. Part (a) exhibits the cluster dioxide and the cluster fragment products. Part (b) shows the cluster monoxide products.

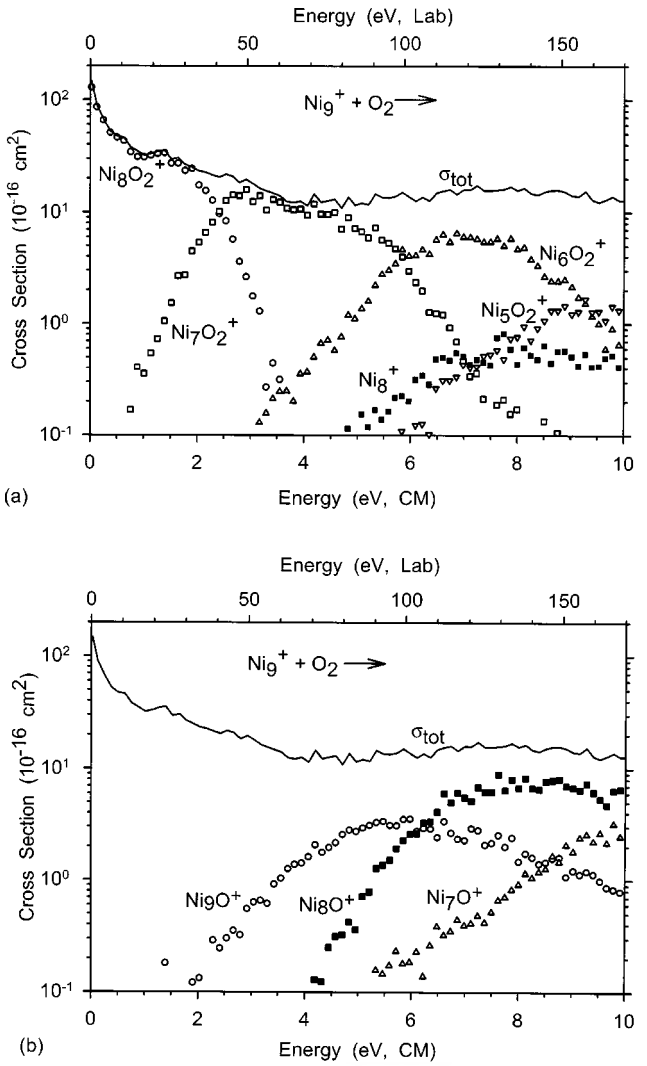

FIG. 5. Cross section for the reaction of Ni_9^+ with O_2 as a function of collision energy in the center-of-mass (lower x axis) and laboratory (upper x axis) frames. Part (a) exhibits the cluster dioxide and the cluster fragment products. Part (b) shows the cluster monoxide products.

third feature beginning near 6 eV corresponds to the dissociation of Ni_4O^+ product by loss of Ni, reaction (18d). The threshold region for Ni_2O^+ clearly corresponds to reaction (19), Ni atom loss from Ni_3O^+ formed in reaction (18a). At higher energies, contributing pathways cannot be determined unambiguously, as the number of neutral products possible increases and the thermochemistry for some of these is not known.

$$Ni_5^+ + O_2 \rightarrow Ni_2O^+ + Ni_2O + Ni. \quad (19)$$

E. $Ni_n^+ + O_2$ (n=6–18)

Although the number of possible reaction products and pathways increases rapidly with increasing reactant cluster size, the reactivity observed actually simplifies and there are strong similarities among the results for the larger clusters. Figures 5 and 6 show results for the reactions of Ni_9^+ and Ni_{16}^+ with dioxygen. These two systems are representative of the behavior of all clusters larger than Ni_5^+. The energy dependences of the reaction cross sections at kinetic energies ranging from thermal up to about 1 eV are comparable to σ_{LGS} for all cluster sizes with magnitudes that are somewhat larger than this prediction.

1. $Ni_mO_2^+$ products

Cluster dioxide ions are the dominant products at low energies, Figs. 5(a) and 6(a). As the cluster reactants increase in size, the energy range over which this is true increases from below about 7 eV for Ni_6^+ to about 9 eV for Ni_{18}^+. It is clear that the cluster dioxides formed at low energies dissociate by sequential loss of nickel atoms as the energy is increased. This is evident from the observation that the cross sections for $Ni_mO_2^+$ products decline as the $Ni_{m-1}O_2^+$ cross sections rise. If there are any features that might correspond to formation of molecular Ni_{n-m} neutrals, they are negligible within our experimental signal to noise ratio. It is also useful to note that because the dissociation processes correspond almost exclusively to $Ni_mO_2^+ \rightarrow Ni_{m-1}O_2^+ + Ni$, this indicates that the ionization energies (IEs) of the larger cluster dioxides must be less than that of atomic Ni.

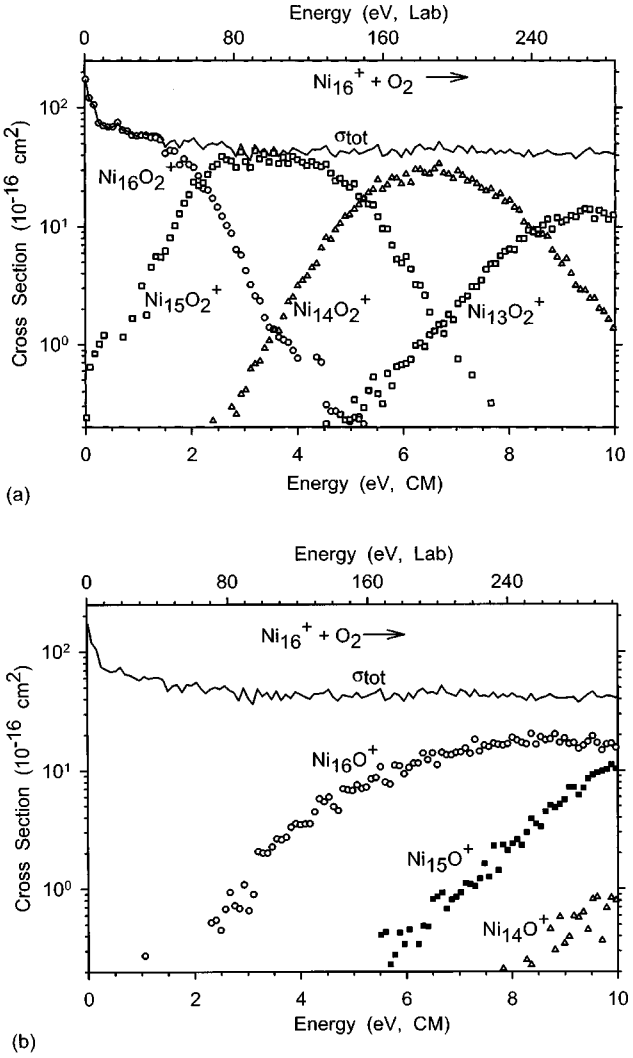

FIG. 6. Cross section for the reaction of Ni_{16}^+ with O_2 as a function of collision energy in the center-of-mass (lower x axis) and laboratory (upper x axis) frames. Part (a) exhibits the cluster dioxide and the cluster fragment products. Part (b) shows the cluster monoxide products.

Although the product distributions are similar for larger clusters, different sized clusters are distinguished by the largest $Ni_mO_2^+$ product (highest m value) observed. This is $Ni_{n-1}O_2^+$ for Ni_4^+ to Ni_9^+. The $Ni_nO_2^+$ adduct is not observed until Ni_{10}^+ and gradually increases in importance until it dominates at low energies for Ni_{12}^+ and larger clusters. These observations are not dependent on the pressure of the O_2 reactant, so that collisional stabilization is not responsible for the $Ni_nO_2^+$ products. As documented below, these changes in the dominant $Ni_mO_2^+$ product observed can be attributed to changes in the thermochemistry of the product species and the increasing lifetimes as the clusters get larger.

2. Ni_mO^+ and Ni_m^+ products

For the Ni_n^+ reactants ($n=6-18$), the Ni_nO^+ product cross sections exhibit thresholds in the vicinity of 1.5–2.5 eV. As the energy is increased, these products dissociate by sequentially losing nickel atoms, Figs. 5(b) and 6(b). We observe that the $Ni_{n-2}O^+$ cross sections show two features for $n \leqslant 12$, as shown for example in Fig. 5(b), in which the second feature begins somewhere near 7 eV. The higher energy feature is clearly a result of concomitant formation of 2 Ni+O, whereas the lower energy feature can be attributed to the formation of NiO+Ni neutral products.

For these larger reactant cluster ions ($n=6-18$), the cluster fragment ions formed in simple CID are minor products. Only the Ni_{n-1}^+ for $n=6$, 9, and 10 ionic products were observed below 10 eV. Other fragments were either not observed or their overall intensity was much less than one percent of all products. Certainly small amounts of such fragments are probably formed but these pathways are not quantitatively important for larger Ni_n^+ clusters.

IV. THERMOCHEMISTRY

A. Threshold analysis

The energy dependence of cross sections for endothermic processes in the threshold region is modeled as detailed in our analogous work on iron cluster reactions with O_2 (Ref. 29) and is outlined in brief here. This procedure uses Eq. (20),[53]

$$\sigma(E) = \sigma_0 \Sigma g_i (E + E_i + E_{\rm rot} - E_0)^N / E, \tag{20}$$

where σ_0 is an energy independent scaling parameter, N is an adjustable parameter, E is the relative kinetic energy, $E_{\rm rot}$ is the average rotational energy of the cluster ion at 300 K, and E_0 is the threshold for the reaction at 0 K. The summation is over the vibrational states i having energies E_i and populations g_i, where $\Sigma g_i = 1$. Vibrational frequencies for the bare cluster ions are obtained as outlined elsewhere[25,40] and use a Debye model.[54] Equation (20) has been used successfully in reproducing the cross sections of various ion–molecule reactions[55] including those of transition metal cluster ions.[25,27–38]

Before we compare the model with the experimental data, several effects are taken into consideration. First, the thermal motion of the target gas and the kinetic energy distribution of the parent ion beam are both convoluted into Eq. (20) as described previously.[41] Second, we extend the range of data analyzed by including a simple statistical model[56] that accounts for the observation that cross sections for both the cluster dioxides and monoxides decline at higher energies because the product dissociates further. Third, the presence of low energy "tails" in some of the experimental cross sections of dioxide products (for $n=6-8$, 15–18), and for monoxide products (for $n=2-5$), which complicate the data analysis, are treated as detailed in our previous work[29] by ignoring the tails, which will tend to give lower limits for E_0. We believe that the uncertainties listed with the threshold values are sufficiently conservative to include errors introduced by ignoring these tails.

Fourth, we account for the possibility that the processes being modeled occur more slowly than the experimental time window available, $\sim 10^{-4}$ s in our apparatus, which results in a delayed onset of the experimental threshold that becomes more significant as the cluster size increases. This is achieved by incorporating RRKM (Rice–Ramsperger–Kassel–Marcus) theory into Eq. (20) as outlined elsewhere.[57] The implementation of RRKM theory in the present work re-

quires the vibrational frequencies of the oxygenated clusters, the reaction degeneracy, and rotational constants for the bare metal and oxygenated clusters, which are chosen in accord with procedures outlined previously.[29] Here, we chose 458 cm^{-1} as the average value for cluster oxygen symmetric and asymmetric stretches and the bend. Conservative errors associated with this estimate were evaluated by multiplying and dividing the frequencies by a factor of 2 and reanalyzing the data. These variations produce differences in the thresholds that are less than 0.02 eV. The choice of the transition state (TS) and its molecular constants parallels those of our previous work[29] and places the TS at the point where the last atom (Ni for all $Ni_mO_2^+$ and $Ni_{n-m}O^+$ products and O for the Ni_nO^+ products) is lost from the oxygenated cluster. The transition state (TS) is assumed to be loose, having molecular constants similar to the dissociated products.[57]

Including these factors, Eq. (20) can accurately model the experimental cross sections from threshold to high energies. The parameters of Eq. (20), σ_0, N, and E_0 are varied until the model reproduces the data optimally as determined by a nonlinear least squares method. Uncertainties in the listed E_0 values include errors associated with variations in E_0 over the range of N values that adequately reproduce several data sets, variations in the vibrational frequencies of the reactant cluster ion by factors of one-half and two, and the absolute uncertainty in the energy scale.

B. Cluster dioxide bond energies, Ni_n^+-2O

1. Qualitative considerations

Before analyzing the endothermic reaction cross sections, it is worth considering the qualitative characteristics of the cluster dioxide product cross sections to obtain some indication of the magnitude of the cluster dioxide bond energies. One key observation is that the formation of the $Ni_{n-2}O_2^+$ cluster is clearly endothermic (or thermoneutral) for all reactant cluster ions larger than four atoms. Therefore, an upper limit to the binding energy of two oxygen atoms to the Ni_{n-2}^+ cluster, $D[Ni_{n-2}^+-2O]$, equals $D(Ni_{n-2}^+-Ni)+D(Ni_{n-1}^+-Ni)+D(O_2)$. Upper limits derived in this manner are listed in Table II. For $n\geqslant 13$, formation of $Ni_{n-1}O_2^+$ also appears to be endothermic, which would suggest that $D[Ni_{n-1}^+-2O]\leqslant D(Ni_{n-1}^+-Ni)+D(O_2)$, values also listed in Table II. It is possible that the appearance of these cross sections is controlled not by the thermodynamics but by the lifetimes of these products. Specifically, this possibility considers that loss of Ni atoms from $Ni_nO_2^+$, $n\geqslant 13$, is still an exothermic process (thermoneutral for $n=12$), but the average time required for this dissociation is longer than the 10^{-4} s available experimentally. However, in the case of iron, chromium, and vanadium cluster reactions,[29–31] the shape of the cross sections proved to be a reliable indicator of the thermochemistry. Lower limits to the Ni_n^+-2O bond energies can be obtained from observations of exothermic reactions. Nickel clusters from $n=4-12$ clearly react exothermically with oxygen to form $Ni_{n-1}O_2^+ + Ni$. This is the most probable reaction product at low energies, accounting for nearly 100% of the total cross section at thermal energies. The lower limits obtained for $D[Ni_{n-1}^+-2O]\geqslant D(Ni_{n-1}^+-Ni)+D(O_2)$ are also listed in Table II. For larger clusters, $n\geqslant 13$, $Ni_nO_2^+$ formation is clearly exothermic, indicating that $D[Ni_n^+-2O]\geqslant D(O_2)$.

TABLE II. Summary of Ni_m^+-2O bond energies (in eV) from several sources.

m	Lower limit[b]	Upper limit[c]	Direct measurement[d]	Relative measurement[e]	Average[f]
3	7.05(0.22)	9.19(0.32)	7.94(0.34)	···	7.94(0.34)
4	7.25(0.23)	9.89(0.34)	8.90(0.39)	8.48(0.58)	8.69(0.35)
5	7.75(0.25)	10.61(0.38)	9.54(0.38)	8.80(0.44)	9.17(0.29)
6	7.97(0.28)	10.51(0.41)	9.26(0.42)	9.04(0.49)	9.15(0.32)
7	7.65(0.30)	10.38(0.44)	9.25(0.45)	8.96(0.55)	9.11(0.36)
8	7.84(0.32)	10.57(0.47)	9.44(0.48)	9.68(0.54)	9.56(0.36)
9	7.84(0.35)	10.67(0.52)	9.12(0.55)	9.40(0.56)	9.26(0.39)
10	7.94(0.39)	11.20(0.55)	8.73(0.55)	9.00(0.55)	8.87(0.39)
11	8.37(0.39)	11.81(0.55)	9.94(0.55)	8.83(0.59)	9.39(0.41)
12	8.55(0.39)	11.44(0.54)	9.47(0.55)	9.06(0.60)	9.27(0.41)
13	5.11(0.002)[g]	11.25(0.55)	9.15(0.56)	9.06(0.57)	9.11(0.40)
14	5.11(0.002)[g]	8.36(0.40)[b]	7.66(0.40)	8.45(0.59)	
	8.36(0.40)	11.66(0.59)	8.93(0.59)	8.82(0.59)	8.88(0.42)
15	5.11(0.002)[g]	8.41(0.43)[b]	7.47(0.43)	8.43(0.62)	
	8.41(0.43)	11.87(0.63)	8.85(0.63)	8.51(0.62)	8.68(0.44)
16	5.11(0.002)[g]	8.57(0.46)[b]	7.53(0.46)	8.02(0.64)	
	8.57(0.46)	11.90(0.57)	8.71(0.60)	8.73(0.64)	8.72(0.44)
17	5.11(0.002)[g]	8.44(0.37)[b]	7.26(0.37)	7.84(0.66)	

[a]Uncertainties in parentheses.
[b]Sum of bond energies for loss of one Ni atom plus $D(O_2)$, except as noted.
[c]Sum of bond energies for loss of two Ni atoms plus $D(O_2)$, except as noted.
[d]Calculated from direct threshold measurements listed in Table III using Eq. (21).
[e]Calculated from relative threshold measurements listed in Table III using Eq. (22).
[f]Average of the direct and relative measurements. Best values.
[g]$D(O_2)$.

2. Direct and relative threshold measurements

Direct measurements of the Ni_n^+-2O bond energies can be obtained by using Eq. (20) to analyze cross sections for cluster dioxides formed in endothermic processes. For smaller clusters, $n=5-15$, the cross sections for the $Ni_{n-2}O_2^+$ product were analyzed. For clusters larger than $n=14$, cross sections for the $Ni_{n-1}O_2^+$ product were also analyzed. The optimized parameters used in Eq. (20) to reproduce the data are listed in Table III and converted to $Ni_{n-x}O_2^+$ thermochemistry by using Eq. (21).

$$D[Ni_{n-x}^+-2O]=D(Ni_{n-x}^+-xNi)+D(O_2)-E_0. \quad (21)$$

The bond energies derived from these direct threshold determinations are listed in Table II to allow comparison between values from different systems and with the upper and lower limits established above. In all cases, there is good agreement between the directly measured bond energies and the upper and lower limits derived from inspection of the data. Bond energies obtained from analyses of $Ni_{n-2}O_2^+$ cross sections exceed those extracted from $Ni_{n-1}O_2^+$ cross sections by an average of 1.33 ± 0.14 eV. In general, bond energies derived from thresholds can be too low for a number of reasons including barriers to the process, competition with other more favorable channels, or kinetic shifts. The only means whereby a threshold can be lower than the true threshold

TABLE III. Summary of parameters used in Eq. (20) for analysis of $Ni_mO_2^+$ cross-sections and relative energy measurements for the dissociation $Ni_mO_2^+ \rightarrow Ni_{m-1}O_2^+ + Ni$.[a]

m	Reactant cluster size, n	σ_0	N	E_0, eV	ΔE, eV[b]
3	5	37.8(13.7)	1.8(0.4)	1.25(0.12)	···
4	6	49.6(3.7)	0.9(0.1)	0.99(0.19)	2.48(0.41)
5	7	14.9(1.8)	1.1(0.1)	1.07(0.06)	2.25(0.13)
6	8	16.9(0.4)	1.5(0.2)	1.25(0.11)	2.51(0.31)
7	9	9.4(2.3)	2.7(0.3)	1.13(0.09)	2.67(0.35)
8	10	23.8(0.3)	2.0(0.1)	1.13(0.10)	3.11(0.27)
9	11	24.6(0.7)	1.4(0.3)	1.55(0.17)	2.57(0.29)
10	12	31.1(4.8)	2.3(0.1)	2.47(0.03)	2.47(0.14)
11	13	35.4(6.3)	2.1(0.2)	1.87(0.04)	2.79(0.22)
12	14	29.7(6.8)	2.1(0.2)	1.97(0.05)	2.93(0.21)
13	15	17.6(6.0)	1.8(0.2)	2.10(0.11)	3.23(0.10)
14	15	46.4(3.7)	1.8(0.1)	0.70(0.03)	2.23(0.21)
14	16	87.6(12)	1.3(0.6)	2.73(0.07)	2.60(0.21)
15	16	53.6(5.7)	1.7(0.1)	0.94(0.02)	2.80(0.22)
15	17	105(6)	1.3(0.1)	3.02(0.07)	2.88(0.22)
16	17	56.9(3.4)	1.9(0.1)	1.04(0.03)	2.64(0.18)
16	18	86.6(9.9)	1.5(0.2)	3.19(0.08)	3.35(0.18)
17	18	54.8(0.1)	1.9(0.1)	1.18(0.02)	2.58(0.16)

[a]Uncertainties in parentheses.
[b]Average of two methods discussed in the text.

(thus giving a bond energy that is too high) is if there are unaccounted sources of energy available, which seems unlikely in these systems. Therefore, the larger bond energies are more likely to be correct, as verified below.

Another way of obtaining information regarding the cluster dioxides is to examine the energy dependence of the $Ni_{n-x}O_2^+$ clusters formed by sequential loss of Ni atoms. The relative thresholds for these reactions can be measured fairly routinely, thereby bypassing questions regarding internal energies of the reactant clusters. Kinetic shifts should also cancel to a large extent although there is the possibility that these differences may represent upper limits to the true thermodynamic differences because of different kinetic shifts for subsequent reactions. Such an interpretation represents a "model free" analysis of the energetics as originally outlined previously.[29]

This analysis was accomplished in two simple ways and relies on the shapes of the $Ni_{n-x}O_2^+$ cross sections being similar in their threshold regions. First, the average energy difference between the cross sections for sequential cluster dioxide products, i.e., $Ni_{n-x}O_2^+$ and $Ni_{n-x-1}O_2^+$, was measured from semilogarithmic plots of the data like those shown in Figs. 3–6 and Ref. 44. Second, cross section data on linear plots was linearly extrapolated to zero cross section and the difference between the intercepts on the energy axis for sequential cluster dioxide products was taken as the energy difference. In both cases, these energy differences, ΔE, correspond to bond energies for $Ni_{n-x-1}O_2^+$–Ni and their averages are listed in Table III. To compare these values to the $Ni_mO_2^+$ thermochemistry obtained above, we convert to $D[Ni_m^+-2O]$ using Eq. (22), where $m=n-x$.

$$D[Ni_m^+-2O]=D(Ni_{m-1}O_2^+-Ni)+D[Ni_{m-1}^+-2O]-D(Ni_{m-1}^+-Ni). \quad (22)$$

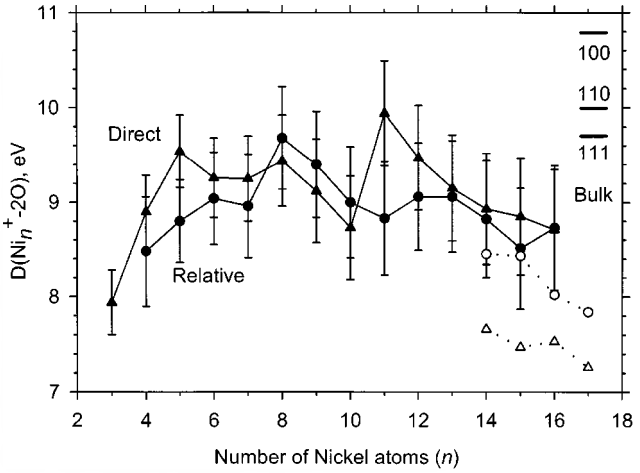

FIG. 7. Comparison of the dioxide bond energies obtained from relative (circles) and direct (triangles) measurements listed in Table II. Solid and open symbols indicate values obtained from analysis of channels involving loss of two and one Ni atoms, respectively. Bulk phase values taken from Ref. 18 for several single crystal surfaces are also indicated.

This equation relies on the Ni_{m-1}^+-2O bond energies for the next smallest cluster, hence, the values listed in Table II derived from these relative threshold measurements are calculated using the average value for the next smallest cluster. This average is calculated from all available values (those directly measured and the relative values). It can be seen that the agreement between the direct and relative measurements is fairly good, generally within the combined experimental errors, Fig. 7. The average value listed in Table II is therefore believed to be our best thermochemical information for the cluster dioxides. For larger clusters, $n \geqslant 14$, the agreement between the direct and relative values is quite good for the bond energies determined from loss of two atoms, with an mean absolute deviation of 0.16 ± 0.17 eV. For bond energies determined from loss of only a single atom, the values are considerably lower and agreement between the direct and relative values is worse, with a mean absolute deviation of 0.71 ± 0.21 eV. As independently noted above, this indicates that the latter values are less accurate than the former. The fact that the former values yield a consistent trend in the Ni_m^+-2O bond energies as a function of cluster size confirms this conclusion.

For $n \leqslant 13$, the average values listed in Table II agree with the limits calculated from loss of one and two nickel atoms being exothermic and endothermic, respectively, helping to confirm the accuracy of these results. For $n > 13$, the average values also fall in the range determined by loss of one and two nickel atoms being exothermic and endothermic, respectively. Thus, the appearances of the $Ni_{n-1}O_2^+$ cross sections for the largest clusters are not good indicators of the endothermicity or exothermicity of the particular process and are influenced by lifetime effects. This conclusion contrasts with our results for iron, vanadium, and chromium cluster ion reactivity with O_2.[29–31]

C. Cluster monoxide bond energies, Ni_n^+-O

1. Qualitative considerations

As a first approximation to the cluster monoxide bond energies, we can assume that the two oxygen bonds in the

TABLE IV. Summary of parameters used in Eq. (20) for the analysis of $Ni_n^+ + O_2 \rightarrow Ni_nO^+ + O$ cross sections and calculated bond energies.[a]

n	σ_0	N	E_0, eV	$D(Ni_n^+-O)$, eV[b]
2	2.8(0.3)	1.0(0.1)	0.37(0.03)	4.74(0.03)
3	0.5(0.4)	2.6(0.3)	0.88(0.14)	4.23(0.14)
4	0.8(0.1)	1.6(0.2)	1.82(0.06)	3.29(0.06)
5	2.0(0.3)	1.0(0.2)	2.12(0.10)	2.99(0.10)
6	1.1(0.5)	1.8(0.1)	2.16(0.05)	2.95(0.05)
7	4.1(0.5)	0.8(0.1)	2.65(0.10)	2.46(0.10)
8	5.1(0.1)	1.4(0.1)	2.63(0.02)	2.48(0.02)
9	1.6(0.3)	2.0(0.2)	2.02(0.11)	3.09(0.11)
10	1.4(0.1)	2.2(0.1)	1.96(0.03)	3.15(0.03)
11	8.4(1.8)	1.4(0.1)	2.38(0.12)	2.73(0.12)
12	3.1(0.5)	1.8(0.1)	1.76(0.07)	3.35(0.07)
13	10.6(1.0)	1.3(0.1)	2.21(0.05)	2.90(0.05)
14	1.8(0.4)	2.2(0.1)	1.50(0.02)	3.61(0.02)
15	2.2(0.3)	2.2(0.1)	1.69(0.04)	3.42(0.04)
16	15.3(1.4)	1.5(0.0)	2.24(0.04)	2.87(0.04)
17	6.3(1.4)	1.8(0.1)	1.99(0.07)	3.12(0.07)
18	16.1(3.8)	1.6(0.1)	2.10(0.08)	3.01(0.08)

[a]Uncertainties in parentheses.
[b]Values are lower limits to true bond energies except for $n=2$ and 3. See text.

TABLE V. Summary of parameters used in Eq. (20) for the analysis of $Ni_{m+1}^+ + O_2 \rightarrow Ni_mO^+ + Ni + O$ cross sections and calculated bond energies.[a]

m	σ_0	N	E_0, eV	$D(Ni_m^+-O)$, eV
1	0.10(0.04)	2.2(0.1)	0.61(0.08)[b]	2.67(0.20)
2	5.6(0.2)	1.4(0.1)	3.12(0.02)	4.36(0.12)
3	6.4(2.8)	1.5(0.2)	3.00(0.44)	4.05(0.49)
4	5.5(1.0)	1.8(0.1)	3.07(0.03)	4.19(0.23)
5	9.4(4.9)	1.5(0.5)	3.32(0.08)	4.43(0.26)
6	5.6(0.3)	1.7(0.1)	3.72(0.04)	4.26(0.28)
7	9.5(3.6)	1.6(0.1)	3.26(0.04)	4.40(0.30)
8	7.0(4.5)	1.7(0.3)	3.87(0.29)	3.97(0.43)
9	5.8(1.7)	1.6(0.2)	3.94(0.12)	3.90(0.37)
10	5.3(0.2)	1.8(0.1)	4.11(0.04)	3.84(0.39)
11	11.5(1.1)	1.8(0.3)	4.12(0.15)	4.25(0.42)
12	4.6(0.1)	1.9(0.1)	4.56(0.06)	4.00(0.40)
13	10.7(1.0)	1.8(0.1)	4.14(0.03)	3.87(0.38)
14	9.9(1.2)	2.0(0.1)	4.36(0.07)	4.00(0.41)
15	14.4(3.6)	1.9(0.1)	4.65(0.11)	3.77(0.44)
16	16.2(1.7)	2.0(0.1)	4.60(0.04)	3.97(0.46)

[a]Uncertainties in parentheses.
[b]Threshold for $NiO^+ + NiO$ formation.

$Ni_nO_2^+$ species are similar, i.e., that $D(Ni_n^+-O)$ is approximately half the $D[Ni_n^+-2O]$ values listed in Table II. This estimate gives Ni_n^+-O bond dissociation energies smaller than $D(O_2)$ for all clusters. This means that formation of Ni_nO^+ in reaction (23)

$$Ni_n^+ + O_2 \rightarrow Ni_nO^+ + O \tag{23}$$

should be endothermic for all clusters, in agreement with our observations, Figs. 1–6 and Ref. 44.

Reactions (23) are analyzed using Eq. (20) and the results given in Table IV. Figure 8 shows that these values fall well below $D(Ni_n^+-2O)/2$ for all clusters but $n=2$ and 3. The Ni_nO^+ species are minor products for most cluster sizes and are in direct competition with formation of the cluster dioxides. The competition between losing an oxygen atom from the $Ni_nO_2^+$ transient intermediate to form the cluster monoxides in reaction (23) and losing a nickel atom, a much more favorable process energetically, probably accounts for the high apparent thresholds observed for the Ni_nO^+ products. It is also possible that there are barriers along the potential energy surface for the oxygen atom loss pathway. In any case, it is clear that the thresholds observed for the $Ni_nO^+ + O$ reaction channel are not reliable measurements of Ni_nO^+ thermochemistry, except possibly for $n=2$ and 3, providing only lower limits.

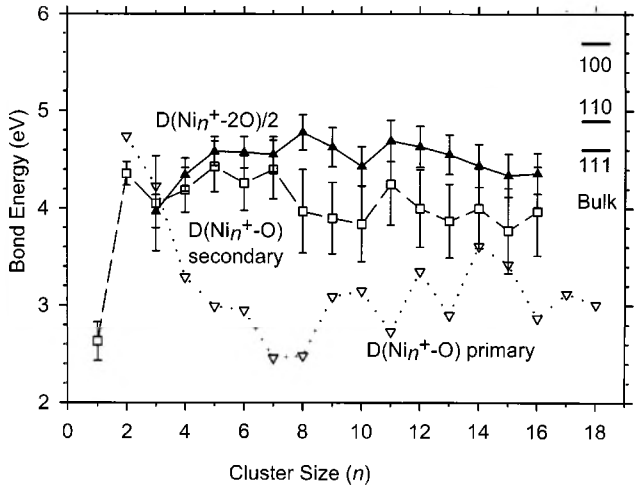

FIG. 8. Comparison of the cluster dioxide bond energies (closed triangles, average values from Table II) with monoxide bond energies obtained from the primary reaction (open triangles, Table IV) and the secondary reaction (open squares, Table V). Bulk phase values taken from Ref. 18 for several single crystal surfaces are also indicated.

2. Direct threshold measurements

The thresholds for reaction (24) provide an alternative method of deriving Ni_n^+-O bond energies,

$$Ni_n^+ + O_2 \rightarrow Ni_{n-1}O^+ + Ni + O. \tag{24}$$

Specifically, the "secondary" bond energies are calculated as $D(Ni_{n-1}^+-O) = D(Ni_{n-1}^+-Ni) - E_0(24) + D(O_2)$, where the bond energies of the bare nickel cluster ions have been measured previously.[25] Here, we determine the thresholds for reaction (24) using an analysis of the cross sections with Eq. (20) as outlined above. The optimized parameters of this model are listed in Table V, along with the bond dissociation energies of Ni_n^+-O obtained from these thresholds using the equation noted above. We also verified that the previously published values of $D_0(Ni_{n-1}^+-Ni)$ could be used in Eq. (20) along with reasonable N values to reproduce the present data for reaction (24), for clusters $n=6$, 9, and 10.

A drawback of measuring thermochemistry in this manner is that the uncertainty is larger because it includes the uncertainties of both reactions (24) and $D(Ni_{n-1}^+-Ni)$. A redeeming feature, however, is that the errors resulting from the kinetic shifts and internal energies should be reduced because identical assumptions are employed for both threshold measurements.

The monoxide bond energy, $D(Ni^+-O)$, obtained from the analysis of the $Ni_2^+ + O_2 \rightarrow NiO^+ + NiO$ secondary reac-

tion, 2.67±0.20 eV, agrees well with the value from the literature, 2.75±0.05 eV (Table I).[45] In the case of $D(Ni_2^+-O)$, the value obtained from the primary reaction exceeds that extracted from the secondary reaction by a considerable amount. Because obtaining a threshold for the latter reaction (9b) requires removing the large exothermic cross section for reaction (9a), it seems likely that the primary bond energy is more reliable. For larger clusters, a comparison of the values from Tables IV and V (see Fig. 8) makes it evident that the primary monoxide bond energies are systematically lower than the secondary bond oxide energies, by an average of 1.04±0.47 eV for $n \geq 4$. Although this discrepancy could be a result of barriers to the primary reaction, such barriers would have to occur in the exit channel as the initial reaction with O_2 is clearly unactivated on the basis of the results for the dioxide products. As loss of a single oxygen atom from $Ni_nO_2^+$ intermediate is unlikely to have a reverse activation barrier, it seems more likely that the low primary monoxide bond energies are the result of thresholds elevated by competition with the much more likely dioxide channels.

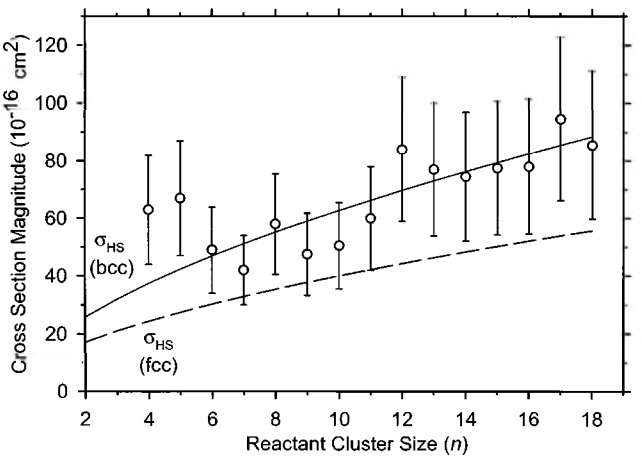

FIG. 9. Comparison of the total reaction cross sections for the reactions of Ni_n^+ ($n=2-18$) with O_2 with 30% uncertainties with the hard sphere limit calculated using Eq. (25) for both a bcc and fcc crystal as a function of cluster size (n). Magnitudes of the total experimental cross sections are averaged over values for energies around 0.5 eV.

V. DISCUSSION

A. Efficiency of reactions

The Langevin–Gioumousis–Stevenson (LGS) expression can often be used to predict the reaction cross section for barrierless, exothermic ion–molecule reactions. Because σ_{LGS} is determined by the polarizability of the neutral gas, it is the same for all cluster ion sizes. Examination of Figs. 1–6 shows that at the very lowest energies, the total reaction cross sections have similar magnitudes and follow an energy dependence that is comparable to $E^{-1/2}$. Within the experimental uncertainties, the cross sections at low energies for all clusters but $n=2$ agree with the calculated collision cross section according to the LGS model, indicating that the reactions occur with unit efficiency at thermal energies. As the energy is increased, however, the total cross sections begin to plateau to a constant value that is maintained to the highest energies examined.

Figure 9 shows the average cross section magnitudes measured experimentally at energies of 0.5 eV along with 30% uncertainties. These values are compared to a hard sphere cross section limit calculated as $\sigma_{HS}=\pi d^2$ where d is the cluster radius plus the dioxygen radius (0.6 Å). The radius of the cluster, r, was estimated using the packing pattern of a cubic crystal and the assumption that the cluster is spherical according to Eq. (25),[29]

$$r=a(3n/4\pi p)^{1/3}, \tag{25}$$

where $a=3.52$ Å,[58] the bulk-phase lattice parameter for nickel, n is the number of nickel atoms, and p is the number of atoms per unit cell: 2 for body-centered cubic (bcc) and 4 for face-centered cubic (fcc). We find better agreement with values calculated for a bcc cell, rather than fcc, even though the bulk-phase structure of nickel metal is fcc at standard conditions. Work by Riley and co-workers has indicated that small nickel clusters have structures based on icosahedra,[59] so there need not be an expectation that the bulk phase geometry is conserved. With the exception of the smallest clusters (where the LGS limit is still being followed), the comparison between σ_{HS} and our experimental cross sections demonstrates that the oxidation reactions of nickel cluster cations with O_2 occur with near unit efficiency that is largely controlled by the size of the cluster at elevated energies.

B. Reaction mechanism

The mechanism for the reactions of nickel cluster ions with O_2 appears fairly straightforward. Dissociative chemisorption of the O_2 molecule on the cluster surface heats the cluster strongly (by 3 to 4.5 eV on the basis of the thermochemistry in Table II) and dissociation ensues. Nickel–oxygen bonds are stronger than nickel–nickel bonds, such that dissociation for larger clusters is dominated by nickel atom loss to form cluster dioxide ions. Formation of primary cluster monoxide products occurs by loss of an oxygen atom, which is less efficient. Competition between these two channels appears to occur early in the reaction scheme, indicating that oxygen atom loss occurs primarily from the transient $Ni_nO_2^+$ intermediate. This seems reasonable as dissociation cools the remaining cluster such that subsequent dissociations must occur primarily along the lowest energy pathways available. In addition to atomic loss processes, loss of molecular products such as NiO and Ni_2O from the transient $Ni_nO_2^+$ can also occur, especially from smaller clusters. Elimination of NiO from the precursor can be readily identified from the exothermic formation of the $Ni_{n-1}O^+$ product for $n=2-4$. As the kinetic energy of the reactants is increased, the primary products dissociate further with loss of atomic nickel again being the most prominent dissociation process for both cluster dioxides and monoxides.

C. Trends in oxygenated nickel cluster stabilities

The various nickel cluster–oxygen bond energies derived above are shown as a function of cluster size in Fig. 8. As found previously for iron, chromium and vanadium clusters,[29–31] it can be seen that the cluster oxygen bond

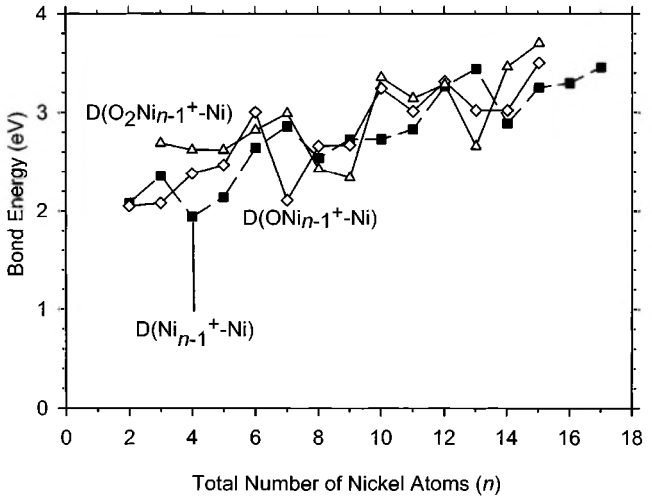

FIG. 10. Comparison of $D(O_xNi_{n-1}^+-Ni)$ for $x=0-2$ as a function of the total number of nickel atoms in the cluster (n). Values for $x=1$ and 2 are calculated using Eq. (26) and those for $x=0$ are taken from Ref. 25.

energies do not vary strongly with cluster size. It can also be seen that the Ni_n^+-O bond energies derived from the secondary $Ni_{n-1}O^+$ product thresholds agree fairly well with half the Ni_n^+-2O bond energies, although the Ni_n^+-O bond energies are systematically lower for clusters larger than $n=4$. For $n\geqslant 8$, the difference is 0.6 ± 0.2 eV, although the combined uncertainties are comparable to this difference. It is possible that these slightly lower bond energies are probably the result of thresholds for formation of $Ni_{n-1}O^+$ shifted to higher energies by competition with the cluster dioxide products. Alternatively, the first oxide bond energy may also reflect the need to distort the nickel cluster to accommodate the oxygen bond. The second bond is stronger because the cluster has already distorted.

Another way to examine the trends in this thermochemistry is to compare the stabilities of bare and oxygenated cluster ions with regard to loss of a nickel atom, the lowest energy dissociation process in all cases. These $O_xNi_{n-1}^+-Ni$ bond energies where $x=1$ and 2 are calculated from Eq. (26),

$$D(O_xNi_{n-1}^+-Ni)=D[Ni_n^+-(O)_x]-D[Ni_{n-1}^+-(O)_x]+D(Ni_{n-1}^+-Ni), \quad (26)$$

where the required bond energies are taken from Tables II, V, and Ref. 25. These comparisons are shown in Fig. 10. For most cluster sizes, the pattern in dissociation energies, $D(O_xNi_{n-1}^+-Ni)$ imitates that for bare clusters, $D(Ni_{n-1}^+-Ni)$. The lack of large changes in the bond energies upon oxygenation simply reflects the fact that the Ni_n^+-2O and Ni_n^+-O bond energies do not change appreciably with cluster size, Fig. 8.

D. Comparison to oxidation of neutral nickel clusters

In flow tube reactor studies on the oxidation of neutral nickel clusters,[60,61] the cluster dioxide products were the first peaks to appear in the mass spectrum. This is consistent with our observation that the cluster dioxide products dominate the spectrum at thermal energies for all but the smallest clusters. These researchers reasoned that the more exothermic addition of O_2 predominates over the approximately thermoneutral addition of a single O atom, as quantified directly here. They also stated that an important cooling mechanism for the oxygenated clusters is by evaporation, as observed directly in the present study.

E. Comparison to bulk phase thermochemistry

Ideally, we would like to compare the bond energies determined here to those on bulk phase Ni surfaces. There have been several studies on the oxidation of single crystal nickel surfaces.[62] The adsorption of O_2 molecular nickel surfaces has been shown to undergo a dissociative chemisorption mechanism.[16] Calorimetry experiments give desorption enthalpies of 4.86 and 4.6 eV for Ni(111), 4.9 eV for Ni(110), and 5.7 eV for Ni(100).[17,18] These bulk phase values are equivalent to Ni_n^+-2O bond energies of in the range of 9.7–10.8 eV, which is comparable to the 7.9–9.6 eV range found here (Table II). This comparison is shown in Figs. 7 and 8. In addition, $\Delta_{vap}H^0(Ni)$ is 4.44 ± 0.09 eV,[53] suggesting that the metal should vaporize before oxygen desorbs for many oxidized nickel surfaces, in agreement with the dissociation behavior observed here. The average (Ni_n^+-2O) bond energy for $n\geqslant 4$ is 9.0 ± 0.4 eV, which is equivalent to a O_2 desorption enthalpy of 3.9 ± 0.4 eV. Thus, the thermochemistry obtained here for small nickel clusters is slightly weaker than that for the bulk phase nickel 111 surface, but not comparable to the 100 surface. This suggests that binding of oxygen in three-fold sites dominates in these small nickel clusters.

ACKNOWLEDGMENTS

This research is supported by the Chemical Sciences, Geosciences, and Biosciences Division, Office of Basic Energy Sciences, U.S. Department of Energy.

[1] M. D. Morse, Chem. Rev. **86**, 1049 (1986); M. M. Kappes, *ibid.* **88**, 372 (1988); D. C. Parent and S. L. Anderson, *ibid.* **92**, 1541 (1992).
[2] M. P. Irion, Int. J. Mass Spectrom. Ion Processes **121**, 1 (1992).
[3] P. B. Armentrout, J. B. Griffin, and J. Conceição, in *Progress in Physics of Clusters*, edited by G. N. Chuev, V. D. Lakhno, and A. P. Nefedov (World Scientific, Singapore, 1999), p. 198; P. B. Armentrout, Annu. Rev. Phys. Chem. **52**, 423 (2001).
[4] J. Conceição, R. T. Laaksonen, L. S. Wang, T. Guo, P. Norlander, and R. E. Smalley, Phys. Rev. B **51**, 4668 (1995).
[5] P. Fayet, M. J. McGlinchey, and L. H. Wöste, J. Am. Chem. Soc. **109**, 1733 (1987).
[6] S. Vajda, S. Wolf, T. Leisner, U. Busolt, and L. H. Wöste, J. Chem. Phys. **107**, 3492 (1997).
[7] M. Ichihashi, T. Hanmura, R. T. Yadav, and T. Kondow, J. Chem. Phys. A **104**, 11885 (2000).
[8] E. K. Parks, K. P. Kerns, and S. J. Riley, J. Chem. Phys. **112**, 3384 (2000).
[9] K. P. Kerns, E. K. Parks, and S. J. Riley, J. Chem. Phys. **112**, 3394 (2000).
[10] P. A. Hintz and K. M. Ervin, J. Chem. Phys. **100**, 5715 (1994).
[11] G. C. Nieman, E. K. Parks, S. C. Richtsmeier, K. Liu, L. G. Pobo, and S. J. Riley, High. Temp. Sci. **22**, 115 (1986).
[12] W. D. Vann, R. L. Wagner, and A. W. Castleman, Jr., J. Phys. Chem. A **102**, 1708 (1998).
[13] W. D. Vann, R. L. Wagner, and A. W. Castleman, Jr., J. Phys. Chem. A **102**, 8804 (1998).

[14] W. D. Vann, R. C. Bell, and A. W. Castleman, Jr., J. Phys. Chem. A **103**, 10846 (1999).
[15] W. D. Vann and A. W. Castleman, Jr., J. Phys. Chem. A **103**, 847 (1999).
[16] *The Chemical Physics of Solid Surfaces and Heterogeneous Catalysis*, Vol. 3a, edited by D. A. King and D. P. Woodruff (North-Holland, Amsterdam, 1990).
[17] J. B. Benziger and R. E. Preston, Surf. Sci. **141**, 576 (1984).
[18] W. A. Brown, R. Kose, and D. A. King, Chem. Rev. **98**, 797 (1998).
[19] L. Lian, C. X. Su, and P. B. Armentrout, J. Chem. Phys. **97**, 4084 (1992).
[20] C. X. Su, D. A. Hales, and P. B. Armentrout, J. Chem. Phys. **99**, 6613 (1993).
[21] C. X. Su, D. A. Hales, and P. B. Armentrout, Chem. Phys. Lett. **201**, 199 (1993).
[22] C. X. Su and P. B. Armentrout, J. Chem. Phys. **99**, 6506 (1993).
[23] L. Lian, C. X. Su, and P. B. Armentrout, J. Chem. Phys. **97**, 4072 (1992).
[24] D. A. Hales, C. X. Su, and P. B. Armentrout, J. Chem. Phys. **100**, 1049 (1994).
[25] L. Lian, C. X. Su, and P. B. Armentrout, J. Chem. Phys. **96**, 7542 (1992).
[26] D. A. Hales, L. Lian, and P. B. Armentrout, Int. J. Mass Spectrom. Ion Processes **102**, 269 (1990).
[27] P. B. Armentrout, D. A. Hales, and L. Lian, in *Advances in Metal and Semiconductor Clusters*, edited by M. A. Duncan (JAI, Greenwich, 1994), Vol. II, p. 1.
[28] P. B. Armentrout, in *Metal–Ligand Interactions—Structure and Reactivity*, edited by N. Russo and D. R. Salahub (Kluwer, Dordrecht, 1996), p. 23.
[29] J. B. Griffin and P. B. Armentrout, J. Chem. Phys. **106**, 4448 (1997).
[30] J. B. Griffin and P. B. Armentrout, J. Chem. Phys. **108**, 8062 (1998).
[31] J. Xu, M. T. Rodgers, J. B. Griffin, and P. B. Armentrout, J. Chem. Phys. **108**, 9339 (1998).
[32] J. B. Griffin and P. B. Armentrout, J. Chem. Phys. **107**, 5345 (1997).
[33] J. B. Griffin and P. B. Armentrout, J. Chem. Phys. **108**, 8075 (1998).
[34] J. Conceição, S. K. Loh, L. Lian, and P. B. Armentrout, J. Chem. Phys. **104**, 3976 (1996).
[35] J. Conceição, R. Liyanage, and P. B. Armentrout, Chem. Phys. **262**, 115 (2000).
[36] R. Liyanage, J. Conceição, and P. B. Armentrout, J. Chem. Phys. **116**, 936 (2002).
[37] F. Liu, R. Liyanage, and P. B. Armentrout, J. Chem. Phys. **117**, 132 (2002).
[38] R. Liyanage, X.-G. Zhang, and P. B. Armentrout, J. Chem. Phys. **115**, 9747 (2001).
[39] F. Liu and P. B. Armentrout (unpublished).
[40] S. K. Loh, L. Lian, and P. B. Armentrout, J. Chem. Phys. **91**, 6148 (1989).
[41] K. M. Ervin and P. B. Armentrout, J. Chem. Phys. **83**, 166 (1985).
[42] E. Teloy and D. Gerlich, Chem. Phys. **4**, 417 (1974); D. Gerlich, Adv. Chem. Phys. **82**, 1 (1992).
[43] N. R. Daly, Rev. Sci. Instrum. **31**, 264 (1959).
[44] See EPAPS Document No. E-JCPSA6-115-009144 for 17 figures. This document may be retrieved via the EPAPS homepage http://www.aip.org/pubservs/epaps.html or from ftp.aip.org in the directory /epaps/. See the EPAPS homepage for more information.
[45] E. R. Fisher, J. L. Elkind, D. E. Clemmer, R. Georgiadis, S. K. Loh, N. Aristov, L. S. Sunderlin, and P. B. Armentrout, J. Chem. Phys. **93**, 2676 (1990).
[46] C. Corliss and J. Sugar, J. Phys. Chem. Ref. Data **11**, 135 (1982).
[47] M. D. Morse, G. P. Hansen, P. R. R. Langridge-Smith, L.-S. Zheng, M. E. Geusic, D. L. Michalopoulos, and R. E. Smalley, J. Chem. Phys. **80**, 5400 (1984).
[48] J. B. Pedley and E. M. Marshall, J. Phys. Chem. Ref. Data **12**, 967 (1983).
[49] W. A. Goddard III, S. P. Walsh, A. K. Rappe, T. H. Upton, and C. F. Melius, J. Vac. Sci. Technol. **14**, 416 (1977).
[50] M. W. Chase, C. A. Davies, J. R. Downey, D. J. Frurip, R. A. McDonald, and A. N. Syverud, J. Phys. Chem. Ref. Data, Suppl. **14**, 1 (1985).
[51] G. Gioumousis and D. P. Stevens, J. Chem. Phys. **29**, 294 (1958).
[52] E. W. Rothe and R. B. Bernstein, J. Chem. Phys. **31**, 1619 (1959).
[53] P. B. Armentrout, in *Advances in Gas Phase Ion Chemistry*, edited by N. G. Adams and L. M. Babcock (JAI, Greenwich, 1992), Vol. I, pp. 83–119.
[54] M. F. Jarrold and J. E. Bower, J. Chem. Phys. **87**, 5728 (1987).
[55] J. L. Elkind and P. B. Armentrout, J. Am. Chem. Soc. **90**, 6576 (1986); P. B. Armentrout, Int. Rev. Chem. Phys. **9**, 115 (1990); in *Advances in Gas Phase Ion Chemistry*, edited by N. G. Adams and L. M. Babcock (JAI, Greenwich, 1992), Vol. I, p. 83; D. E. Clemmer, Y.-M. Chen, N. Aristov, and P. B. Armentrout, J. Phys. Chem. **98**, 7538 (1994).
[56] M. E. Weber, J. L. Elkind, and P. B. Armentrout, J. Chem. Phys. **84**, 1521 (1986).
[57] M. T. Rodgers, K. M. Ervin, and P. B. Armentrout, J. Chem. Phys. **106**, 4499 (1997).
[58] C. Kittel, *Solid State Physics* (Wiley, New York, 1976).
[59] E. K. Parks, L. Zhu, J. Ho, and S. J. Riley, J. Chem. Phys. **100**, 7206 (1994); *ibid.* **102**, 7377 (1995).
[60] S. J. Riley, E. K. Parks, G. C. Nieman, L. G. Pobo, and S. Wexler, J. Chem. Phys. **80**, 1360 (1984); G. C. Nieman, E. K. Parks, S. C. Richtsmeier, K. Liu, L. G. Pobo, and S. J. Riley, High. Temp. Sci. **22**, 115 (1986).
[61] R. L. Whetten, D. M. Cox, D. J. Trevor, and A. Kaldor, J. Phys. Chem. **89**, 566 (1985).
[62] C. N. R. Rao, V. Vijayakrishnan, G. U. Kulkarni, and M. K. Rajumon, Appl. Surf. Sci. **84**, 285 (1995).